Letter

Field-induced chiral soliton phase in the Kitaev spin chain

Erik S. Sørensen [1,*] Jacob Gordon,[2] Jonathon Riddell,[1] Tianyi Wang [2] and Hae-Young Kee [2,3,†]

[1]*Department of Physics & Astronomy, McMaster University, Hamilton, Ontario, Canada L8S 4M1*

[2]*Department of Physics, University of Toronto, Ontario, Canada M5S 1A7*

[3]*Canadian Institute for Advanced Research, CIFAR Program in Quantum Materials, Toronto, Ontario, Canada M5G 1M1*

(Received 12 September 2022; accepted 6 February 2023; published 27 February 2023)

The bond-dependent Ising interaction present in the Kitaev model has attracted considerable attention. The appearance of an unexpected intermediate phase under a magnetic field is particularly intriguing, and one may wonder if a similar phase occurs in the Kitaev spin chain with alternating x- and y-bond Ising interactions. Previous studies have focused on a transverse field h_z and reported a direct transition to the polarized state. Here, we investigate phases with an arbitrary angle of two longitudinal fields, h_x and h_y. For a magnetic field applied along the diagonal, $h_x = h_y$, the chain remains gapless up to a critical field h_{xy}^{c1}. Surprisingly, above h_{xy}^{c1} it enters an unusual intermediate phase before reaching the polarized state at h_{xy}^{c2}. This phase is characterized by a staggered vector chirality and for periodic boundary conditions, a twofold degeneracy with a finite gap. For open boundary systems the ground state exhibits a single *soliton*, lowering the energy, and in-gap excitations. However, the corresponding antisoliton raises the energy sufficiently that a gap appears for soliton and antisoliton pairs in periodic systems. An intuitive variational picture is developed describing the soliton phase. A phase descending from the intermediate field phase is also identified in the two-leg Kitaev ladder.

DOI: 10.1103/PhysRevResearch.5.L012027

Introduction. The Kitaev model, characterized by the bond-dependent Ising spin interaction in a honeycomb lattice [1], has recently generated considerable interest, as it offers a rare quantum spin liquid as an exact ground state. Among several exotic phenomena discussed in relation to the extended Kitaev model [2], the proposed field-induced $U(1)$ spin liquid in the antiferromagnetic (AFM) Kitaev model under a magnetic field is especially fascinating [3–5]. While the mechanism of the $U(1)$ spin liquid is still missing, a magnetically disordered phase featuring a staggered scalar chirality has been found in the quasi-one-dimensional AFM Kitaev ladder under a [111] magnetic field [6]. The relation between these phases, if any, is at present not clear and a detailed understanding of the field-dependent phase diagram as the two-dimensional limit is approached, starting from the purely one-dimensional (1D) Kitaev spin chain, would clearly be desirable. This then raises the question if any nontrivial phases exist for the Kitaev spin chain in a magnetic field.

The 1D Kitaev $s = \frac{1}{2}$ spin chain has been investigated and shown to map to a free-fermion model [7–11]. With the Kitaev chain defined in terms of x- and y-bond Ising interactions, it has been shown that under a transverse magnetic field h_z, the model directly enters the polarized state without any phase transition [8]. In fact, so far no intermediate phase in an applied field has been reported for the Kitaev spin chain. One may then wonder if the Kitaev spin chain exhibits any intermediate phase under a magnetic field such as the ladder and C_3 symmetric honeycomb lattice mentioned above. Here,

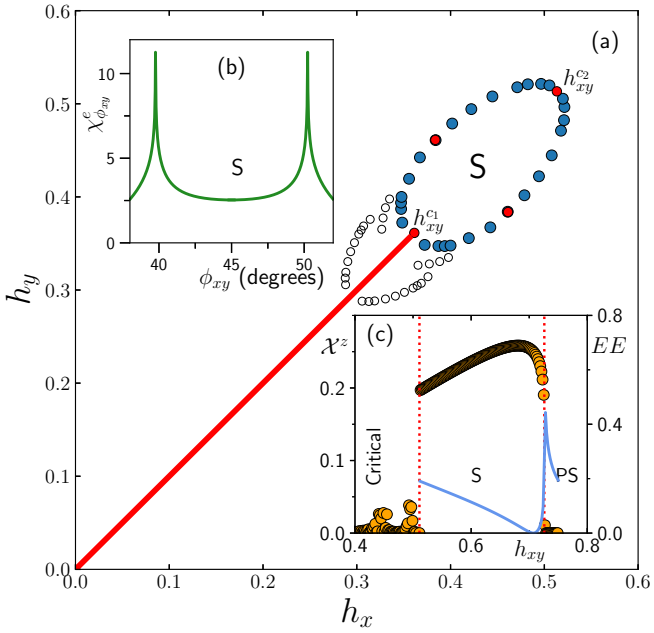

FIG. 1. (a) The phase diagram in the (h_x, h_y) plane from ED, $N = 24$ (solid blue points), iDMRG (solid red points). The soliton phase is marked by an "S." Open circles indicate crossover observed in ED due to incommensurability effects. (b) iDMRG results for $\chi^e_{\phi_{xy}}$ at $|h| = 0.6$ vs ϕ_{xy}. (c) $\mathcal{X}^z$ vs h_{xy} at a field angle to 45° from iDMRG (orange points) and the bipartite entanglement entropy EE (blue line).

*sorensen@mcmaster.ca

†hykee@physics.utoronto.ca

we address this question, and report an unusual intermediate chiral phase possessing magnetic solitons in the AFM Kitaev spin chain under a magnetic field close to the $h_x \sim h_y$. This phase is absent in the ferromagnetic (FM) Kitaev spin chain.

The $s = \frac{1}{2}$ Kitaev spin chain is described by the Hamiltonian

$$\mathcal{H} = K \sum_j \left(S^x_{2j+1} S^x_{2j+2} + S^y_{2j+2} S^y_{2j+3} \right) - \sum_j \boldsymbol{h} \cdot \boldsymbol{S}_j, \quad (1)$$

where we set $g = \hbar = \mu_B = 1$ and consider the AFM model with $K = 1$ and a parametrization of the field term as $\boldsymbol{h} = h(\cos\phi_{xy}\cos\theta_z, \sin\phi_{xy}\cos\theta_z, \sin\theta_z)$. We refer to the coupling KS^xS^x as an x bond (_) and KS^yS^y as a y bond (..). Below, we determine the phase diagram of Eq. (1) in a field using Lanczos exact diagonalization (ED) techniques in combination with density matrix renormalization group (DMRG) and infinite-size DMRG (iDMRG) [12–15] methods typically performed with a bond dimension larger than 1000 and $\epsilon < 10^{-10}$. Subsequently, we describe our variational calculations valid in the chiral soliton phase.

Phase diagram. In the presence of a field in the z direction, the Kitaev chain Eq. (1) is exactly solvable and it is known that the system immediately enters the polarized state (PS) [8] directly. The integrability is lost when the field is applied in the x or equivalently the y direction and the situation is less clear. We have therefore studied the correlation functions $C(r) = \langle S^x_1 S^x_{r+1} \rangle$ for small fields in the x direction. For $h_x = 0$ a power law is found, $C(r) \sim r^{-0.25(1)}$, as shown in the Supplemental Material [16], however, for any nonzero h_x an exponential decay is observed with a resulting finite gap [16]. The polarized state is then entered directly for any nonzero h_x and by symmetry for any nonzero h_y.

Next we study the phase diagram for fields in the entire x-y plane [Fig. 1(a)]. Although difficult to establish numerically, our results indicate that for $\phi_{xy} = 45^\circ$ the Kitaev chain remains gapless up to a critical field $h^{c_1}_{xy} = 0.511K$ where a new unexpected phase is entered, marked by "S." We determine the phase boundary for this phase by studying the energy susceptibility $\chi^e_{\phi_{xy}} = -\partial^2 e_0 / \partial \phi^2_{xy}$ which scales as $N^{2/\nu-(d+z)}$ at a quantum critical point [17]. Here, e_0 is the energy per site and ν, z the correlation and dynamical exponents. The solid blue points denote results from $N = 24$ ED where $\chi^e_{\phi_{xy}}$ is maximal. The positions of these peaks are confirmed by iDMRG (solid red points) as illustrated in Fig. 1(b). The open circles denote crossover due to incommensurability effects where the position of the ED peak cannot be reproduced with iDMRG and is strongly finite-size dependent. The phase extends out of the x-y plane to nonzero θ_z [16]. At a 45° angle another quantum critical point is observed at the critical field $h^{c_2}_{xy} = 0.726K$ where the chain transitions from the soliton phase to the polarized state.

The gapless phase, extending from zero field to $h^{c_1}_{xy}$ at a 45° angle, is a critical *line*. For $\phi_{xy} \neq 45^\circ$, or $\theta_z \neq 0$, a gap opens up and the chain enters the PS phase. The S phase is characterized by a nonzero staggered vector chirality $\mathcal{X}^\alpha$,

$$\mathcal{X}^\alpha = (-1)^j \langle (\mathbf{S}_j \times \mathbf{S}_{j+1})^\alpha \rangle. \quad (2)$$

While $\mathcal{X}^{x,y} = 0$ in the S phase $\mathcal{X}^z \neq 0$ as shown in Fig. 1(c). In the context of the anisotropic J_1-J_2 model with $J_1 < 0$, $J_2 > 0$ [18–20] phases with nonzero $\mathcal{X}^\alpha$ have been found and recently observed in the $s = \frac{1}{2}$ chain $LiCuVO_4$ [21].

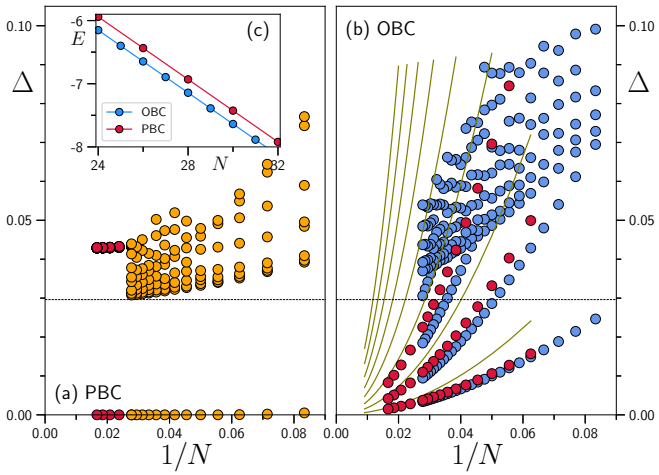

FIG. 2. Energy gap Δ to the first ten energy levels above the ground state (not shown) vs $1/N$ at $h_{xy} = 0.7$. (a) ED results with PBC for even $N = 12$–36 (orange points). Note the twice degenerate ground state below a well-defined gap. The dashed line indicates $\Delta_{\rm PBC} = 0.02962K$. Two soliton variational results (red points). (b) ED results with OBC for $N = 12$–36 (blue points). Variational estimates for the lowest gaps in the space of single defects (green lines) and with $\{0, 1, 2\}$ defects (red points). (c) ED results for the ground-state energy vs N at $h_{xy} = 0.7$, for OBC (blue) and PBC (red).

To understand the nature of the unexpected S phase we focus on the spectrum of excitations. Using ED for chain sizes ranging from $N = 12$ to 36 at $h_{xy} = 0.7$, $\phi_{xy} = 45^\circ$, $\theta_z = 0^\circ$ results for the gap to the ten lowest states are shown in Fig. 2(a) for periodic boundary conditions (PBCs) (orange points) and Fig. 2(b) for open boundary conditions (OBCs) (blue points). For PBCs there are *two* almost degenerate states that become degenerate as $N \to \infty$ below a well-defined but small gap of $\Delta_{\rm PBC} = 0.02962K$. For PBC we determine the momentum of the lowest excited state above the two degenerate ground states to be at $k = 0$. For OBC the spectrum is more intriguing. As seen in Fig. 2(b) the spectrum evolves smoothly with N for both even and odd N. While it is possible to identify $\Delta_{\rm PBC}$ in the spectrum for OBC an increasing number of states appear *below* this gap, quickly approaching the ground-state energy. Counterintuitively, as shown in Fig. 2(c), the ground-state energy is *always lower* for OBC as compared to PBC for any N, despite the missing bond. At $h_{xy} = 0.7$ we determine $\Delta_{\rm O-PBC} = -0.2121K$. Open boundary conditions therefore allow the chain to significantly lower the energy. The proliferation of states below the gap for OBC is an unusual feature reflecting the excited states of the soliton, as we discuss below.

The ground-state magnetization $\langle S^\alpha_i \rangle$ is very unique in the S phase for OBC. As seen in Figs. 3(b) and 3(c), $\langle S^\alpha_i \rangle$ (shown only for *odd* sites) alternates between the x and y directions with a single twist, a *topological soliton*, occurring in the middle of the chain. For $h_{xy} < h^{c_1}_{xy}$ the on-site magnetization is much more complicated and five crossings are present for $N = 384$. In the PS phase for $h_{xy} > h^{c_2}_{xy}$ the spins simply

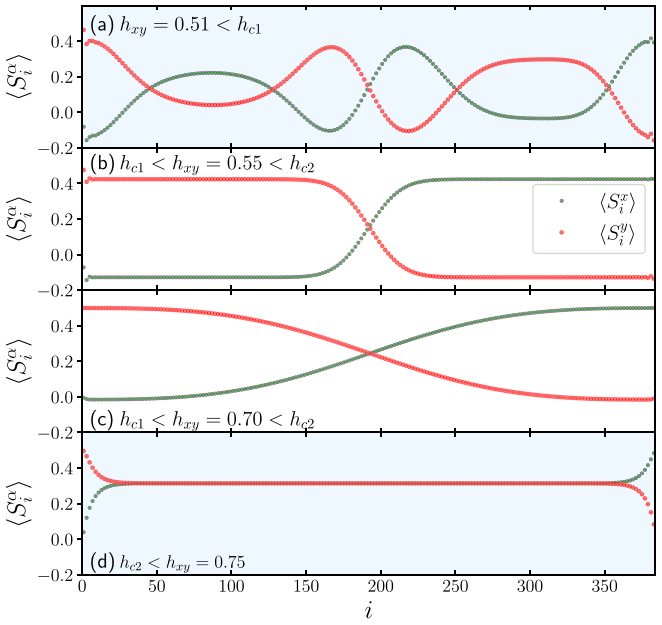

FIG. 3. (a)–(d) Finite chain DMRG results for the on-site magnetization $\langle S_i^x \rangle$, $\langle S_i^y \rangle$ vs position i for an $N = 384$ site chain with OBC at different field strengths. (a) $h_{xy} = 0.51 < h_{c1}$, (b) $h_{xy} = 0.55$, (c) $h_{xy} = 0.70$, (d) $h_{xy} = 0.75 > h_{xy}^{c2}$. Only *odd* sites are shown.

align with the field and the soliton is absent. A useful way to visualize the solitons is to plot the energy density for each bond e_i. In the bulk this is just a constant, e_0^{YX}, but the presence of the soliton *lowers* e_i below this value, locally. This is shown in Fig. 4(b) where $\langle e_i \rangle - e_0^{YX}$ is plotted versus i for $h_{xy} = 0.6$, showing a sharply localized soliton. If we now evaluate

$$\Delta_b = \sum_i \left(\langle e_i \rangle - e_0^{YX} \right), \tag{3}$$

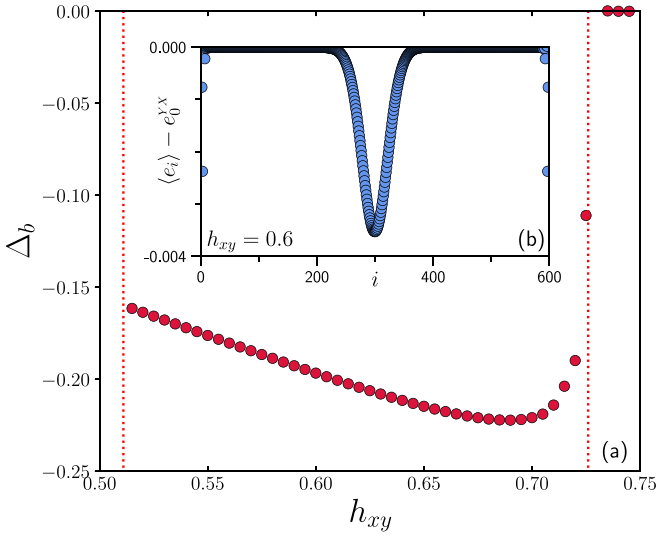

FIG. 4. (a) $N = 1200$ DMRG results with OBC for the soliton mass, Δ_b vs h_{xy} at $\phi_{xy} = 45°$. (b) $\langle e_i \rangle - e_0^{YX}$ vs i at $h_{xy} = 0.6$, $\phi_{xy} = 45°$.

we can determine by how much the soliton has lowered the total energy which we denote as the soliton mass Δ_b. Results for Δ_b calculated this way are shown in Fig. 4(a) throughout the soliton phase. While closely related, $\Delta_{\mathrm{O-PBC}}$ includes boundary effects from the missing bond with OBC.

Variational picture, PBC. As shown in Fig. 1(c) the entanglement entropy (EE) is relatively low in the soliton phase. In fact, for PBC and N even the twofold degeneracy noted in the ground-state subspace in Fig. 2(a) is closely described by two (zero-defect) *product* states of the following form,

$$|X'Y'\rangle = |x'y'x'y'\cdots\rangle, \quad |Y'X'\rangle = |y'x'y'x'\cdots\rangle, \tag{4}$$

where $|y'\rangle = (e^{-i(\pi/2+c)}, 1)/\sqrt{2}$, $|x'\rangle = (e^{ic}, 1)/\sqrt{2}$. The $|x'\rangle$ and $|y'\rangle$ are eigenstates of $\vec{S} \cdot \vec{n}_\alpha$ where the unit vectors $\vec{n}_{x'}$, $\vec{n}_{y'}$ are close to the x and y directions but *crucially* with an angle between them exceeding $\pi/2$, by $2c$. The usual $|x\rangle$ and $|y\rangle$ states are obtained by setting $c = 0$. The optimal value for c depends on the field h_{xy} and is determined in the Supplemental Material [16] to be $c = \cos^{-1}(h_{xy}/K) - \pi/4$. The solitons shown in Figs. 3(b) and 3(c) for OBC then interpolate between these two degenerate states as is typical for *topological* solitons [22]. Although $\langle X'Y'|H|Y'X'\rangle$ is nonzero for very short chains this coupling quickly goes to zero with N.

OBC, any N. We now focus on OBC irrespective of N, and we focus exclusively on the case where the chain *starts with* an $S_1^x S_2^x$ term (▬), in which case the solitons in Fig. 3 transition from the $y'x'$ to the $x'y'$ pattern. Within the soliton phase the lowest-energy subspace is well described by linear combinations of (single defect) states of the form

$$\begin{aligned} |\psi_b(i)\rangle &= |y'▬ x'\cdots y'▬ \overbrace{x_i'\cdots x'}▬ y'\cdots x'▬ y'\cdots x'▬ y'\rangle, \\ |\psi_b(i)\rangle &= |y'▬ x'\cdots y'▬ x'\cdots \overbrace{y_i'▬ y'}\cdots x'▬ y'\cdots x'▬ y'\rangle, \end{aligned} \tag{5}$$

transitioning from the $y'x'$ to the $x'y'$ pattern at bond i. Note that, even though $x_i'\cdots x'$ have the spins aligned ferromagnetically along x, it costs little energy since it occurs on a y bond. Similarly, the spins at $y_i'▬ y'$ are aligned ferromagnetically along y, but on an x bond. Analogously, we can define "antidefects" of the form

$$\begin{aligned} |\psi_B(i)\rangle &= |x'▬ y'\cdots x'▬ \boxed{y_i'\cdots y'}▬ x'\cdots y'▬ x'\cdots y'▬ x'\rangle, \\ |\psi_B(i)\rangle &= |x'▬ y'\cdots x'▬ y'\cdots \boxed{x_i'▬ x'}\cdots y'▬ x'\cdots y'▬ x'\rangle, \end{aligned} \tag{6}$$

in this case transitioning from the $x'y'$ to the $y'x'$ pattern at bond i. Contrary to the defects, ψ_b, these antidefects are relatively *costly* since $y_i'\cdots y'$ now occurs on a y bond and $x_i'▬ x'$ on an x bond.

The states ψ_b and ψ_B are not eigenstates of the Hamiltonian [16] but we expect linear combinations of the single defect $|\psi_b(i)\rangle$ to realistically define the low-energy subspace of the system in a variational manner. We therefore define the (single defect) soliton states:

$$|\Psi_b\rangle = \sum_k a_k |\psi_b(k)\rangle. \tag{7}$$

Similarly, we can define $|\Psi_B\rangle = \sum c_l |\psi_B(l)\rangle$ but this leads to *high*-energy states. It is important to note that the states $|\psi_b(i)\rangle$, while normalized, are not orthogonal. Due to the

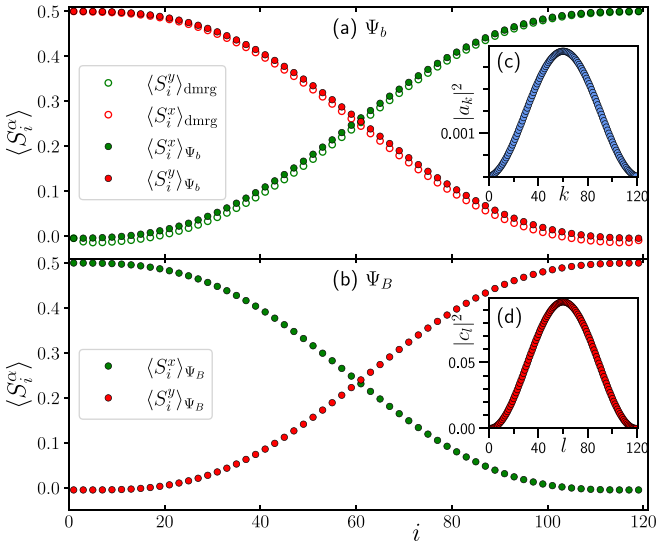

FIG. 5. (a) $\langle S_i^x\rangle$ and $\langle S_i^y\rangle$ on *odd* sites from DMRG calculations on an $N = 120$ site open chain compared to the variational results $\langle S_i^x\rangle_{\Psi_b}$, $\langle S_i^x\rangle_{\Psi_b}$ in the variational soliton state Ψ_b at $h_{xy} = 0.7$, $\phi_{xy} = 45^\circ$. (b) $\langle S_i^x\rangle_{\Psi_B}$, $\langle S_i^x\rangle_{\Psi_B}$ on *odd* sites in the variational "antisoliton" state Ψ_B. (c) $|a_k|^2$ vs k for the Ψ_b state. (d) $|c_l|^2$ vs l for the Ψ_B state.

nonorthogonality, determining the optimal values for the coefficients a_k in Ψ_b in Eq. (7) from a variational calculation therefore defines a generalized eigenvalue problem in terms of the matrices $\mathcal{H}_{kl} = \langle\psi_b(k)|H|\psi_b(l)\rangle$ and $\mathcal{S}_{kl} = \langle\psi_b(k)|\psi_b(l)\rangle$, with similar definitions for the state Ψ_B. The generalized eigenvalue problem can be solved using standard methods and the optimal Ψ_b and Ψ_B determined.

Variational results. Solving the generalized eigenvalue problem yields a series of states for Ψ_b and Ψ_B. With OBC we expect the lowest Ψ_b state to be a good approximation to the ground state. This is illustrated in Figs. 5(a) and 5(c) where the variational results for $\langle S_i^{x,y}\rangle_{\Psi_b}$ are compared to finite chain DMRG results for a system with $N = 120$ at $h_{xy} = 0.7$. We find $E_{\rm DMRG} = -29.9169$ while $E_{\Psi_b} = -29.9019$ less than 0.05% higher. For comparison, the defect-free $Y'X'$ state has an energy $E_{Y'X'} = -29.6975$ significantly higher and the soliton has therefore *lowered* the energy with respect to the $Y'X'$ state. However, for the "antisoliton" state Ψ_B shown in Figs. 5(b) and 5(d) we instead find $E_{\Psi_B} = -29.4520$ *above* the $Y'X'$ state. Using the defect-free $Y'X'$ state as a reference we can now estimate the energy difference (mass) for the two states at $h_{xy} = 0.7$: $\Delta_b = -0.2044K$ compared to $-0.2085K$ from DMRG in Fig. 4(a) and $\Delta_B = 0.2455K$ which cannot be determined from DMRG or ED. A similar asymmetry has been noted in the Rice-Mele model [23] and the nonsymmorphic symmetry [24] present also in the Kitaev spin chain could be crucial.

For PBCs the ground state in the soliton phase is well described by the degenerate and defect-free $Y'X'$ and $X'Y'$ states. While for OBC the number of solitons $n_{\rm sol}$ can be both even and odd, with PBC it is not possible to consider a single soliton, because they have to come in a bB pair or multiple pairs, 0, bB, $bBbB$, ..., with $n_{\rm sol}$ *even*. This explains the gap seen in Fig. 2(a) since to a first approximation we expect that

$$\Delta_{\rm PBC} = \Delta^b + \Delta^B, \tag{8}$$

which would predict a gap for PBC of $0.0411K$ from the variational results. For OBC the gap to the lowest bBb state from the b ground state should then also be equal to $\Delta_{\rm PBC}$, which agrees with the results in Fig. 2(b). We then extend the variational calculations to two-defect bB states by considering

$$|\psi_{bB}(i,j)\rangle = |y'\!-\!\overbrace{x_i'..x'}\!-\!y'..x'\!-\!y'..\boxed{x_j'\!-\!x'}..y'\!-\!x'\rangle, \tag{9}$$

and defining two-soliton states of the form

$$|\Psi_{bB}\rangle = \sum_{i\neq j} a_{i,j}|\psi_{bB}(i,j)\rangle. \tag{10}$$

If we include the $Y'X'$ and $X'Y'$ states in the variational calculation, extending the subspace to $\{0, 2\}$ defects, we find at $h_{xy} = 0.7$ a gap of $\Delta_{\rm PBC}^{\rm var} = 0.04289K$ [red circles in Fig. 2(a)], in qualitative agreement with the ED result of $\Delta_{\rm PBC} = 0.02962K$ and close to $\Delta_b + \Delta_B$. We expect the inclusion of multiple pairs of defects in the variational subspace to further improve the agreement. We can now intuitively understand the transition at $h_{xy}^{c_1}$. At this point $\Delta_b = -\Delta_B$ and the cost of a bB pair becomes zero. As is clearly seen in Fig. 3(a), a number of bB pairs then condense into the single soliton ground state, in this case creating a $bBbBb$ state. As the field is increased the solitons then effectively *evaporate*. On the other hand, the transition at $h_{xy}^{c_2}$ occurs due to the closing of the gap to spin-wave excitations.

The solution of the generalized eigenvalue problem leads not only to the variational ground state Ψ_b but also a series of excitations of these states, ${}^i\Psi_b$, which are in good agreement with results for excited states obtained from DMRG [16]. For OBC, these states correspond to static excitations of the single soliton present in the system [25]. As the system size is increased the excited states gradually fill in the gap in the spectrum. The variationally determined gaps obtained from the single defect states [Eq. (5)] are shown as the green lines in Fig. 2(b). For short chains with OBC we can extend the variational subspace in Eq. (7) to include $\{0, 1, 2\}$ defects with the resulting gaps shown as red circles in Fig. 2(b) significantly improving the agreement with the ED results for short chains.

Discussion. In parallel with studies of solitons in conducting polymers [26], magnetic solitons have been studied since the late 1970s [27–32] with signatures observed experimentally [33] in the 1D easy-plane ferromagnetic chain system $CsNiF_3$ as well as the 1D AFM materials tetramethylammonium manganese trichloride (TMMC) [34,35], $CsCoBr_3$ [36], and $CsMnBr_3$ [37], among others. The excitations of interest here are topological solitons linking distinguishable ground states [22]. Building on this picture, domain walls between degenerate ground states in dimerized spin chains, such as the $s = \frac{1}{2}$, J_1-J_2 model, have been viewed as solitons [38–43] and observed experimentally in $BiCu_2PO_6$ above a critical field [44]. Comparing periodic (PBC) and open (OBC) boundary conditions, a *positive* mass Δ_s has then been defined [41–43] for both the soliton and antisoliton in the dimerized phase with a well-defined spin, $s = \frac{1}{2}$.

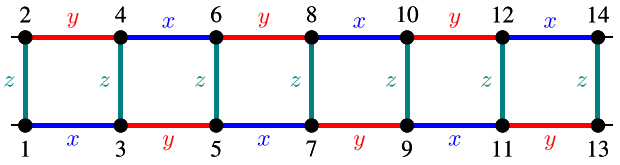

FIG. 6. The Kitaev ladder with colors indicating x, y, and z bonds.

In contrast, for the Kitaev chain we find here that the soliton mass Δ_b is *negative*, lowering the energy in the soliton phase, while the antisoliton has *positive* mass, raising the energy by Δ_B, more than compensating the soliton. In periodic systems, the low-lying excitation, a pair of solitons and antisolitons, then has a small gap given by the difference between Δ_B and Δ_b. At h_{xy}^{c1} the two masses cancel out, $\Delta_b = -\Delta_B$. Furthermore, the soliton and antisoliton do not have a well-defined spin.

Several important tasks remain to be addressed in future work. One is finding candidate Kitaev spin chain systems. Recently, $CoNb_2O_6$ was proposed as a twisted Kitaev chain [45]. However, the Kitaev interaction is FM and finding an AFM sister material would be of considerable interest. Preliminary results for the AFM twisted Kitaev chain show that the phase diagram is similar to the Kitaev chain considered here [16]. Furthermore, an understanding of the dynamics of the solitons in a nonequilibrium setting and their signature in thermodynamic properties such as the specific heat should be developed. Another task is the connection, if any, of the soliton phase to the puzzling intermediate field-induced $U(1)$ spin liquid reported in a finite cluster study of the two-dimensional AFM Kitaev model under a field [3]. As a first step in this direction, we have studied the two-leg Kitaev ladder,

$$H_{\text{Ladder}} = \sum_{\langle i,j\rangle_{\gamma\in(x,y,z)}} K S_i^\gamma S_j^\gamma - \sum_j \boldsymbol{h}\cdot\boldsymbol{S}_j, \qquad (11)$$

where $\gamma = x/y/z$, and $\langle i, j\rangle$ refers to the nearest-neighbor sites. Apart from the x and y bonds occurring in the Kitaev chain, the ladder now also includes z-Ising interactions and we may view the Hamiltonian as shown in Fig. 6. In the presence of a field in the [111] direction the ladder has been extensively studied [6,46] with the antiferromagnetic Kitaev phase (AK) appearing for $K > 0$ and the polarized state (PS) at high fields. Intriguingly, if instead a field is applied in the h_x, h_y plane, two phases which we denote D (for defect) and D′ can be identified [16] in the Kitaev ladder by studying χ_h^e, with the D phase appearing between $h_{xy}/K = 0.402$ and 0.583 for a field in the [110] direction. The phase diagram in the h_x, h_y plane is shown in Fig. 7(a). The D phase is dominated by physics closely resembling that of the soliton phase of the Kitaev chain. This can be seen in Fig. 7(b) where $\langle S_i^{x,y}\rangle$ is plotted along one leg of a 400-site ladder showing a defect in the middle of the ladder strikingly similar to the solitons observed in the chain. However, in this case the defect is not simply a transition between the $Y'X'$ and $X'Y'$ states but displays a more intricate transition between patterns with a period of 6. This is reflected in the ground-state degeneracy for PBC, which in the D phase shows a threefold degeneracy

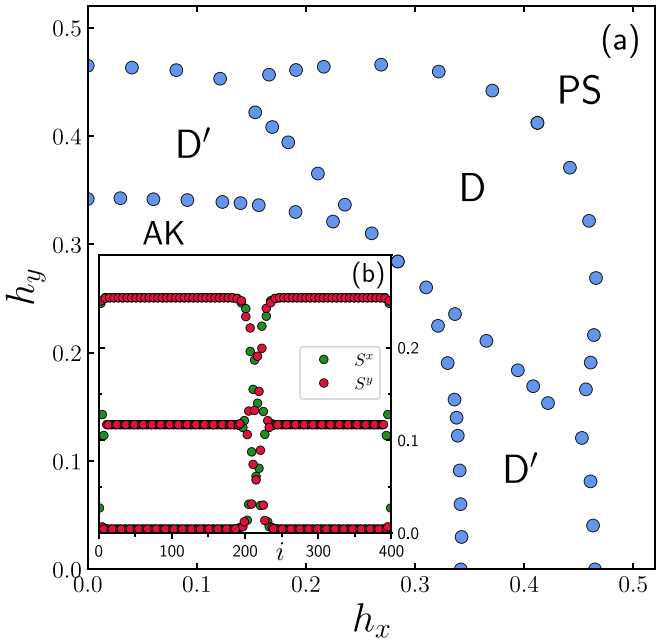

FIG. 7. (a) The phase diagram of an $S = 1/2$ Kitaev ladder in the h_x, h_y plane obtained from iDMRG. The phase marked D is the phase dominated by ground-state defects shown in (b). The phase denoted D′ is a closely related defect phase with a unique ground state. AK denotes the Kitaev phase and PS the polarized state. (b) $\langle S_i^{x,y}\rangle$ from $N = 400$ finite chain DMRG calculations at $h[110] = 0.46K$ with a field in the [110] direction. Results are shown for one leg of the ladder with every point plotted. $\langle S_i^z\rangle$ (not shown) is uniformly zero.

with a gap to excited states. In contrast, the D′ phase with PBC has a unique ground state with a gap and is therefore distinct from the D phase. As was the case for the soliton phase in the Kitaev chain, the D phase extends out in the h_x, h_y plane away, as shown in Fig. 7(a). By symmetry, results along the [110], [$\bar{1}\bar{1}$0], and [$\bar{1}$10] directions are identical. While it is tempting to connect the D and D′ phases to the field-induced phase in two dimensions as the number of legs grows, a future study with a systematic increase of the number of legs is needed.

Acknowledgments. We acknowledge the support of CIFAR and the Natural Sciences and Engineering Research Council of Canada (NSERC) through Discovery Grants (No. RGPIN-2017-05759 and No. RGPIN-2022-04601). H.-Y.K. acknowledges the support by the Canada Research Chairs Program. Computations were performed in part on the GPC and Niagara supercomputers at the SciNet HPC Consortium. SciNet is funded by the Canada Foundation for Innovation under the auspices of Compute Canada, the Government of Ontario, Ontario Research Fund - Research Excellence, and the University of Toronto. Computations were also performed in part by support provided by SHARCNET (www.sharcnet.ca) and Compute/Calcul Canada (www.computecanada.ca). Part of the numerical calculations were performed using the ITensor library [15].

[1] A. Y. Kitaev, Anyons in an exactly solved model and beyond, Ann. Phys. **321**, 2 (2006).

[2] J. G. Rau, E. K.-H. Lee, and H.-Y. Kee, Generic Spin Model for the Honeycomb Iridates beyond the Kitaev Limit, Phys. Rev. Lett. **112**, 077204 (2014).

[3] C. Hickey and S. Trebst, Emergence of a field-driven $U(1)$ spin liquid in the Kitaev honeycomb model, Nat. Commun. **10**, 530 (2019).

[4] H.-C. Jiang, C.-Y. Wang, B. Huang, and Y.-M. Lu, Field induced quantum spin liquid with spinon Fermi surfaces in the Kitaev model, arXiv:1809.08247.

[5] L. Zou and Y.-C. He, Field-induced QCD_3-Chern-Simons quantum criticalities in Kitaev materials, Phys. Rev. Res. **2**, 013072 (2020).

[6] E. S. Sørensen, A. Catuneanu, J. S. Gordon, and H.-Y. Kee, Heart of Entanglement: Chiral, Nematic, and Incommensurate Phases in the Kitaev-Gamma Ladder in a Field, Phys. Rev. X **11**, 011013 (2021).

[7] X.-Y. Feng, G.-M. Zhang, and T. Xiang, Topological Characterization of Quantum Phase Transitions in a Spin-1/2 Model, Phys. Rev. Lett. **98**, 087204 (2007).

[8] K.-W. Sun and Q.-H. Chen, Quantum phase transition of the one-dimensional transverse-field compass model, Phys. Rev. B **80**, 174417 (2009).

[9] N. Wu and W.-L. You, Exact zero modes in a quantum compass chain under inhomogeneous transverse fields, Phys. Rev. B **100**, 085130 (2019).

[10] W.-L. You, Y. Wang, T.-C. Yi, C. Zhang, and A. M. Oles, Quantum coherence in a compass chain under an alternating magnetic field, Phys. Rev. B **97**, 224420 (2018).

[11] L. C. Wang and X. X. Yi, Geometric phase and quantum phase transition in the one-dimensional compass model, Eur. Phys. J. D **57**, 281 (2010).

[12] S. R. White, Density Matrix Formulation For Quantum Renormalization Groups, Phys. Rev. Lett. **69**, 2863 (1992).

[13] I. P. McCulloch, Infinite size density matrix renormalization group, revisited, arXiv:0804.2509.

[14] U. Schollwöck, The density-matrix renormalization group in the age of matrix product states, Ann. Phys. **326**, 96 (2011).

[15] M. Fishman, S. R. White, and E. M. Stoudenmire, The ITensor software library for tensor network calculations, arXiv:2007.14822.

[16] See Supplemental Material at http://link.aps.org/supplemental/10.1103/PhysRevResearch.5.L012027 for additional information about the results presented in the main paper.

[17] A. F. Albuquerque, F. Alet, C. Sire, and S. Capponi, Quantum critical scaling of fidelity susceptibility, Phys. Rev. B **81**, 064418 (2010).

[18] S. Furukawa, M. Sato, Y. Saiga, and S. Onoda, Quantum fluctuations of chirality in one-dimensional spin-1/2 multiferroics: Gapless dielectric response from phasons and chiral solitons, J. Phys. Soc. Jpn. **77**, 123712 (2008).

[19] S. Furukawa, M. Sato, and S. Onoda, Chiral Order and Electromagnetic Dynamics in One-Dimensional Multiferroic Cuprates, Phys. Rev. Lett. **105**, 257205 (2010).

[20] S. Furukawa, M. Sato, S. Onoda, and A. Furusaki, Ground-state phase diagram of a spin-$\frac{1}{2}$ frustrated ferromagnetic XXZ chain: Haldane dimer phase and gapped/gapless chiral phases, Phys. Rev. B **86**, 094417 (2012).

[21] C. P. Grams, D. Brüning, S. Kopatz, T. Lorenz, P. Becker, L. Bohatý, and J. Hemberger, Observation of chiral solitons in $LiCuVO_4$, Commun. Phys. **5**, 37 (2022).

[22] T. Dauxois and M. Peyrard, *Physics of Solitons* (Cambridge University Press, Cambridge, UK, 2006).

[23] R. E. J. Allen, H. V. Gibbons, A. M. Sherlock, H. R. M. Stanfield, and E. McCann, Nonsymmorphic chiral symmetry and solitons in the Rice-Mele model, Phys. Rev. B **106**, 165409 (2022).

[24] W. Yang, C. Xu, S. Xu, A. Nocera, and I. Affleck, Nonsymmorphic Luttinger liquids in the generalized antiferromagnetic kitaev spin-1/2 chain, arXiv:2202.11686.

[25] R. Rajaraman, *Solitons and Instatons* (North-Holland, Amsterdam, 1987).

[26] A. J. Heeger, S. Kivelson, J. R. Schrieffer, and W. P. Su, Solitons in conducting polymers, Rev. Mod. Phys. **60**, 781 (1988).

[27] H. J. Mikeska, Solitons in a one-dimensional magnet with an easy plane, J. Phys. C **11**, L29 (1978).

[28] H. J. Mikeska, Non-linear dynamics of classical one-dimensional antiferromagnets, J. Phys. C **13**, 2913 (2000).

[29] H. C. Fogedby, Solitons and magnons in the classical Heisenberg chain, J. Phys. A: Math. Gen. **13**, 1467 (1980).

[30] H. C. Fogedby, The spectrum of the continuous isotropic quantum Heisenberg chain: Quantum solitons as magnon bound states, J. Phys. C **13**, L195 (1980).

[31] A. Kosevich, B. Ivanov, and A. Kovalev, Magnetic solitons, Phys. Rep. **194**, 117 (1990).

[32] H.-J. Mikeska and M. Steiner, Solitary excitations in one-dimensional magnets, Adv. Phys. **40**, 191 (1991).

[33] J. K. Kjems and M. Steiner, Evidence for Soliton Modes in the One-Dimensional Ferromagnet $CsNiF_3$, Phys. Rev. Lett. **41**, 1137 (1978).

[34] J. P. Boucher, F. Mezei, L. P. Regnault, and J. P. Renard, Diffusion of Solitons in the Antiferromagnetic Chains of $(CD_3)_4NMnCl_3$: A Study by Neutron Spin Echo, Phys. Rev. Lett. **55**, 1778 (1985).

[35] L. P. Regnault, J. P. Boucher, J. Rossat-Mignod, J. P. Renard, J. Bouillot, and W. G. Stirling, A neutron investigation of the soliton regime in the one-dimensional planar antiferromagnet $(CD_3)_4NMnCl_3$, J. Phys. C **15**, 1261 (1982).

[36] W. J. L. Buyers, M. J. Hogan, R. L. Armstrong, and B. Briat, Solitons in the one-dimensional Ising-like antiferromagnet $CsCoBr_3$, Phys. Rev. B **33**, 1727 (1986).

[37] B. D. Gaulin and M. F. Collins, Evidence for out-of-easy-plane solitons in $CsMnBr_3$, Can. J. Phys. **63**, 1235 (1985).

[38] B. S. Shastry and B. Sutherland, Excitation Spectrum of a Dimerized Next-Neighbor Antiferromagnetic Chain, Phys. Rev. Lett. **47**, 964 (1981).

[39] W. J. Caspers and W. Magnus, Some exact excited states in a linear antiferromagnetic spin system, Phys. Lett. A **88**, 103 (1982).

[40] W. J. Caspers, K. M. Emmett, and W. Magnus, The Majumdar-Ghosh chain. twofold ground state and elementary excitations, J. Phys. A: Math. Gen. **17**, 2687 (1984).

[41] E. Sørensen, I. Affleck, D. Augier, and D. Poilblanc, Soliton approach to spin-Peierls antiferromagnets: Large-scale numerical results, Phys. Rev. B **58**, R14701 (1998).

[42] E. S. Sørensen, M.-S. Chang, N. Laflorencie, and I. Affleck, Impurity entanglement entropy and the Kondo screening cloud, J. Stat. Mech. (2007) L01001.

[43] E. S. Sørensen, M.-S. Chang, N. Laflorencie, and I. Affleck, Quantum impurity entanglement, J. Stat. Mech. (2007) P08003.

[44] F. Casola, T. Shiroka, A. Feiguin, S. Wang, M. S. Grbić, M. Horvatić, S. Krämer, S. Mukhopadhyay, K. Conder, C. Berthier, H.-R. Ott, H. M. Rønnow, C. Rüegg, and J. Mesot, Field-Induced Quantum Soliton Lattice in a Frustrated Two-Leg Spin-1/2 Ladder, Phys. Rev. Lett. **110**, 187201 (2013).

[45] C. M. Morris, N. Desai, J. Viirok, D. Huvonen, U. Nagel, T. Room, J. W. Krizan, R. J. Cava, T. M. McQueen, S. M. Koohpayeh, R. K. Kaul, and N. P. Armitage, Duality and domain wall dynamics in a twisted Kitaev chain, Nat. Phys. **17**, 832 (2021).

[46] A. Catuneanu, E. S. Sørensen, and H.-Y. Kee, Nonlocal string order parameter in the $S = \frac{1}{2}$ Kitaev-Heisenberg ladder, Phys. Rev. B **99**, 195112 (2019).